# Coordinated Resource Allocation-Based Integrated Visible Light Communication and Positioning Systems for Indoor IoT

Helin Yang<sup>®</sup>, Student Member, IEEE, Wen-De Zhong, Senior Member, IEEE, Chen Chen<sup>®</sup>, Member, IEEE, Arokiaswami Alphones<sup>®</sup>, Senior Member, IEEE, Pengfei Du<sup>®</sup>, Sheng Zhang<sup>®</sup>, and Xianzhong Xie<sup>®</sup>, Member, IEEE

Abstract-With the rapid development of Internet of Things (IoT) in the smart city, smart grid and smart industry, indoor communication and positioning are important fields of applications for indoor IoT. This paper presents an integrated visible light communication and positioning (VLCP) system for indoor IoT, in order to provide the high-speed data rate and high-accuracy positioning for IoT devices. where the filter bank multicarrier-based subcarrier multiplexing (FBMC-SCM) technique is exploited to effectively reduce the out-of-band interference (OOBI) on both adjacent communication and positioning subcarriers. After that, we propose a coordinated resource allocation approach for the system with the purpose of maximizing the sum rate while guaranteeing the minimum data rates and positioning accuracy requirements of devices. To this end, we solve the optimization problem by decomposing it into two subproblems, where a low-complexity suboptimal subcarrier allocation approach is proposed and the sequential quadratic programming (SQP) method is adopted to solve the non-linearly constrained power allocation optimization problem. Numerical results verify the superiority in performance of the presented integrated VLCP system for indoor IoT, and the results

Manuscript received September 11, 2019; revised January 13, 2020; accepted April 2, 2020. Date of publication April 14, 2020; date of current version July 10, 2020. This work was support in part by the Delta-NTU Corporate Lab for Cyber-Physical Systems from Delta Electronics Inc., in part by the National Research Foundation Singapore through the Corporation Lab University Scheme, in part by the National Natural Science Foundation of China under Grant 61901065 and Grant 61502067, in part by the Key Research Project of Chongqing Education Commission under Grant KJZD-K201800603, in part by the Key Project of Science and Technology Research of Chongqing Education Commission under Grant KJZD-M201900602, and in part by the Chongqing Nature Science Foundation under Grant CSTC2018jcyjAX0432 and Grant CSTC2016jcyjA0455. This article was presented at the IEEE International Conference on Communications (ICC), Shanghai, China, May 2019. The associate editor coordinating the review of this article and approving it for publication was Y. Shen. (Corresponding author: Chen Chen.)

Helin Yang, Wen-De Zhong, Arokiaswami Alphones, and Sheng Zhang are with the School of Electrical and Electronic Engineering, Nanyang Technological University (NTU), Singapore 639798 (e-mail: hyang013@e.ntu.edu.sg)

Chen Chen is with the School of Microelectronics and Communication Engineering, Chongqing University, Chongqing 400044, China (e-mail: c.chen@cqu.edu.cn).

Pengfei Du is with the A\*STAR's Singapore Institute of Manufacturing Technology, Singapore 138632.

Xianzhong Xie is with the Chongqing Key Lab of Computer Network and Communication Technology, Chongqing University of Posts and Telecommunications, Chongqing 400065, China.

Color versions of one or more of the figures in this article are available online at http://ieeexplore.ieee.org.

Digital Object Identifier 10.1109/TWC.2020.2986109

also reveal that the proposed coordinated resource allocation approach can effectively improve the sum rate and the positioning accuracy compared with other resource allocation approaches.

Index Terms—Internet of Things, visible light communication and positioning, multi-cell, filter-bank multicarrier, coordinated resource allocation.

#### I. INTRODUCTION

NTERNET of Things (IoT) has been emerging as a promising vision for the next generation networks through realizing the smart manufacturing, smart grid, and smart city [1], [2]. However, with the advanced wireless communication, more and more smart devices are involved in IoT, resulting in the radio frequency (RF) spectrum scarcity. Moreover, some indoor IoT devices need the high positioning accuracy where indoor RF-based localization systems are still inaccurate and unreliable in indoor IoT due to the multipath reflections and shadowing [3], [4].

Recently, light emitting diodes (LEDs) have achieved much attention recently in the lighting market and will replace traditional light sources for its long lifetime, low power consumption, faster switching time and reliability [5]. Besides illumination, LEDs are also used for visible light communications (VLC) and visible light positioning (VLP) [3], [5]. VLC and VLP based on white LEDs have gained much attention for their wide applications such as homes, supermarket, hospital, airplanes and industry [3], [5].

On the one hand, VLC based on white LEDs has been emerging as a promising candidate for indoor wireless communication systems due to its many attractive characteristics, such as economic, abundant unregulated bandwidth and high security [5]. From now on, some studies [6]–[9] have adopted VLC for indoor IoT networks to support the high data transmission rates and guarantee different quality-of service (QoS) requirements of IoT devices. Considering that there exists energy-constrained IoT devices, the literatures [6] and [7] proposed the light energy harvesting models to support both the communication services and energy harvesting purposes, where the energy from light signals is harvested by IoT devices over VLC downlinks and the harvested energy is used for the data transmissions over RF links. Moreover, the hybrid

1536-1276 © 2020 IEEE. Personal use is permitted, but republication/redistribution requires IEEE permission. See https://www.ieee.org/publications/rights/index.html for more information.

VLC/RF IoT networks were presented to offer the better service to devices [8], [9], where the VLC network can support the high data rate and the RF network guarantees the seamless coverage.

Furthermore, considering that the practical VLC system generally has multiple optical attocells, resource allocation in multi-cell VLC systems has also been investigated [10]–[15]. In [10] and [11], a multiple access resource allocation approach was proposed to manage the inter-cell interference (ICI) under both the interference and power constraints in multi-cell VLC systems. Moreover, coordinated resource allocation approaches have been proposed to effectively mitigate ICI or improve the resource utilization performance in downlink multi-cell VLC systems [12], [13]. By taking devices' locations into account, joint device association/grouping and power allocation approaches have been studied to improve the system performance by mitigating ICI in multi-cell VLC systems [14], [15].

On the other hand, VLP has become an attractive research typical recently, because it provides the high positioning accuracy and guaranteed security compared with the RF based indoor positioning systems [3], [16]-[21]. Many algorithms have been proposed in indoor VLP systems, such as received signal strength (RSS), angle of arrival (AOA), time difference of arrival (TDOA), and phase difference of arrival (PDOA) [16]-[21]. The literatures in [16] and [17] experimentally evaluated real-time localization schemes using the RSS algorithm for the IoT devices with the high positioning accuracy, but RSS has low estimation accuracy when the device locates at the edges of a room. In particular, Zhang et al. experimentally evaluated a high positioning accuracy scheme based on AOA, but it needs a highly complicated image sensor arrays [18]. In [19] and [20], authors presented modified PDOA schemes with low complexity to improve the positioning accuracy and experimental results indicated that the high positioning accuracy achieved by using the two schemes. Moreover, the studies in [21] and [22] investigated the multi-path reflections effect on the positioning accuracy performance of in VLP based positioning systems, and advanced methods were proposed to mitigate a part of multipath reflections. Compared with RSS, TOA and AOA, the accuracy of TDOA and PDOA relates to the sampling rate at receivers and these two approaches have high positioning accuracy [3], but TDOA requires high time resolution due to the short distance between transmitters and receivers in indoor environments, so that PDOA is more appropriate in indoor VLP systems [19], [20] and will be applied in our developed system. In addition, we would like to mention that only a few works investigating power allocation among LED transmitters in VLP systems [23]–[25].

However, most of the works just only focused on VLC [6]–[15] or VLP independently [16]–[24]. In practical indoor environments, such as office, hospital and industry, both communication and positioning services might be expected at the same time. So far, only several works considered the integration of VLC and VLP for both communication and positioning purposes [18], [26], where the combination of OFDM modulation and RSS algorithm has been proposed for the

integration of VLC and VLP. In addition, an integrated VLC and VLP (VLCP) system using filter bank multicarrier-based subcarrier multiplexing (FBMC-SCM) and PDOA was proposed in [27], which can effectively reduce the out-of-band interference (OOBI) instead of using a amounts of frequency spacing as guard bands (GBs) between two adjacent subbands to avoid OOBI. Hence, not only does FBMC improve the positioning accuracy and effective subcarrier utilization ratio in integrated VLCP systems by reducing OOBI, but also enhances the spectral efficiency [1], [27]. Unfortunately, the above integrated VLCP systems [18], [26], [27] did not investigate the resource allocation for both communication and positioning scenarios under practical optical constraints, which still remains a significant challenge, especially in multi-cell IoT systems.

To address the above-mentioned issues, this paper presents an integrated VLCP system for indoor IoT, with the objective of supporting the high-speed data rate and high-accuracy positioning services. A joint coordinated subcarrier and power allocation approach is firstly proposed in multi-cell integrated VLCP systems, in order to maximize the system data rate while guaranteeing the minimum data rate and positioning accuracy requirements of IoT devices. The main contributions of our works can be summarized as follows:

- In order to provide the high-speed data rate and high-accuracy positioning services for indoor IoT devices, an integrated VLCP system is proposed in this paper. Then, we study the optimization problem of joint subcarrier and power allocation in coordinated multi-cell integrated VLCP systems by considering the unique practical optical constraints, i.e., the limited liner optical power range of LED lamps, the non-negative transmitted signal in VLCP systems and the different QoS requirements, which are very different from RF communication systems.
- We solve the optimization problem by decomposing it into two subproblems, i.e., subcarrier allocation and power allocation, which can be solved iteratively. In the first subproblem, a low-complexity suboptimal subcarrier allocation approach is proposed to guarantee the minimum rate requirements of devices first, and then allocate the remaining subcarriers to optimize the system sum rate. Considering that the second subproblem is non-convex with non-linear constraints, the sequential quadratic programming (SQP) method is adopted to solve the non-linearly constrained power allocation optimization problem.
- We analyze the principle of the multi-cell integrated VLCP system with two modulation schemes, i.e., FBMC-SCM and OFDM-SCM, and evaluate the performance of our proposed resource allocation approach from the perspectives of system sum rate and positioning accuracy under different scenarios. Numerical results verify the feasibility of our proposed approach for multi-cell integrated VLCP systems.

The rest of this paper is organized as follows. In Section II, we describe the presented integrated VLCP system model for indoor IoT. Section III introduces the system constraints

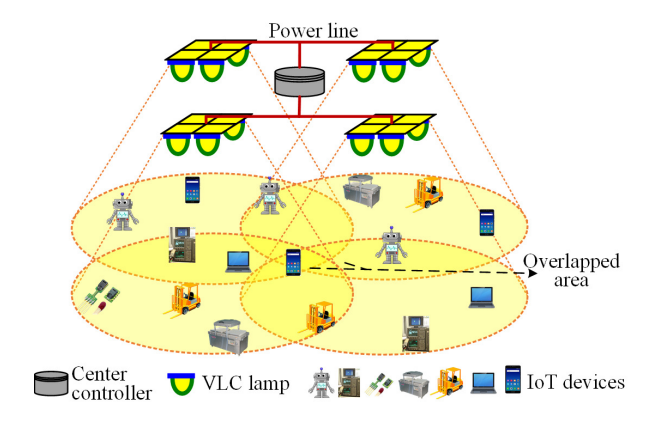


Fig. 1. An indoor multi-cell integrated VLCP system for IoT devices.

and formulates the optimization problem. The solution to the resource allocation problem is provided in Section IV. The numerical results and discussions are provided in Section V. Finally, conclusions are shown in Section VI.

#### II. INTEGRATED VLCP SYSTEM FOR INDOOR IOT

#### A. System Model

We consider a downlink multi-cell integrated VLCP system, as illustrated in Fig. 1, where each cell is formed by M LED lamps and a number of IoT devices (K devices) are randomly located on the floor in the room. Note that to the best of our knowledge, there is no study on the in multi-cell integrated VLCP system. For easy presentation, this paper takes four cells as an example to provide our investigation on the multi-cell integrated VLCP system. In addition, we would like to mention that our presented work can be extended to a large-scale indoor room with more cells. In addition to offer the lighting requirements, the system provides both communication and positioning services for devices. We assume that there exists a central controller in the system [24], which connects all LED lamps to broadcast information to devices simultaneously. We assume that the uplink feedback is provided by the WiFi links and each cell can share the feedback information with other cells through the central controller. After receiving the feedback information, the central controller can tackle resource allocation. Each device is equipped with one photodiode (PD) and the total bandwidth is equally divided into  $N (N = N_{po} + N_{co})$  subcarriers with  $N_{po}$  subcarriers being used for the PDOA positioning and  $N_{co}$  subcarriers being served for communication.

In order to improve the subcarrier utilization, the system adopts the unity frequency reuse (UFR) design in the multicell integrated VLCP system, where the communication subcarriers are reused across all cells. In this paper, let  $\mathcal{M}_c$  denotes the set of all the LED lamps in cell c, let  $\mathcal{K}$  denotes the set of devices, let  $\mathcal{N}_{c,\text{co}}$  and  $\mathcal{N}_{c,\text{po}}$  denote the sets of the communication subcarriers and the subcarriers used for positioning subcarriers in cell c, respectively.

At the m-th LED lamp in cell c, the transmitted data  $z_{c,m}$  is a linear combination of the devices' communication data flow and the sinusoidal positioning data flow, which can be given

as

$$z_{c,m} = \sum_{k \in \mathcal{K}} \sum_{n \in \mathcal{N}_{c,co}} \rho_{k,c,n}^{\text{co}} \sqrt{P_{m,c,n}^{\text{co}}} s_{k,c,n}^{\text{co}} + \sqrt{P_{m,c,i}^{\text{po}}} s_{c,i}^{\text{po}} + A$$

$$\tag{1}$$

where  $\rho_{k,c,n}^{\rm co}$  denotes a binary variable,  $\rho_{k,c,n}^{\rm co} \in \{0,1\}$ , and  $\rho_{k,c,n}^{\rm co} = 1$  represents the n-th communication subcarrier of cell c is allocated to the k-th device; otherwise, it takes the value 0.  $P_{m,c,n}^{\rm co}$  and  $P_{m,c,i}^{\rm po}$  indicate the allocated transmit electrical power on the n-th communication subcarrier and on the i-th positioning subcarrier at the m-th LED lamp in cell c, respectively.  $s_{k,c,n}^{\rm co}$  is the communication data for the k-th device, on the n-th subcarrier in cell c, and  $s_{c,i}^{\rm po}$  is the positioning data on the i-th subcarrier in cell c, and we set that the mean of  $s_{k,c,n}^{\rm co}$  or  $s_{c,i}^{\rm po}$  is zero, and they are in the range of  $[-\sigma,\sigma]$  with  $\sigma>0$  [10], [29]. A denotes the direct current (DC) offset which is added to ensure that the transmitted signal is non-negative and guarantee the illumination (brightness levels) requirement in the room. Through a biastee, the alternating-current (AC) signal is mixed with DC bias and finally modulated on the LED lamps.

For the optical link, the line-of-sight (LOS) channel gain from one LED lamp to one device is expressed as

$$h = \begin{cases} \frac{(\vartheta + 1)A_r}{2\pi d^2} \cos^{\vartheta}(\phi) T_s(\psi) g(\psi) \cos \psi, & 0 \le \psi \le \psi_c \\ 0 & \psi_c < \psi \end{cases}$$
(2)

where  $A_r$  is the active area of the PD. d and  $\psi$  denote the distance and the angle of incidence between the LED and the device, respectively.  $\phi$  is the angle of irradiance from the LED to the device.  $\vartheta$  denotes the order of Lambertian emission, which is given by  $\vartheta = -\ln 2/(\ln \cos \phi_{1/2})$  with  $\phi_{1/2}$  being the LED's semi-angle at half power.  $T_s(\psi)$  and  $g(\psi)$  are the gain of the optical filter and the optical concentrator gain at the PD, respectively, where  $g(\psi)$  can be expressed as:  $g(\psi) = \eta/\sin^2\!\psi_c$ , where  $\eta$  is the refractive index.  $\psi_c$  stands for the semi-angle field of view (FOV) of the PD.

In complex indoor environments, the received signals at the PD through diffuse path may suffer from multipath propagation which causes inter symbol interference (ISI) [20]–[22], [29]. We would like to mention that ISI arriving from LED lamps will degrade both the communication and positioning performance, which need to be considered in practical integrated VLCP systems.

Hence, in integrated VLCP systems, the received signals suffer from multipath propagation which causes ISI. In this paper, let  $\delta_{\rm ISI}^2$  denote the ISI noise power caused by the multipath propagation, which can be expressed as [30]

$$\delta_{\rm ISI}^2 = \mu^2 P_{\rm r, ISI}^2 \tag{3}$$

In (3),  $P_{r,ISI}$  denotes the received ISI power which can be calculated according to the study [30].

In this case, the dominant noise contribution at the receiver can be expressed as

$$\delta^2 = \delta_{\text{shot}}^2 + \delta_{\text{thermal}}^2 + \delta_{\text{ISI}}^2 \tag{4}$$

where  $\delta_{\rm back}^2$  and  $\delta_{\rm ISI}^2$  are the background noise and the ISI noise, respectively. In addition,  $\delta_{\rm back}^2$  is the additive white Gaussian noise (AWGN) power. The more details about the above mentioned multipath channel can be found in the literatures [26], [30]. We would like to mention that for the multipath channel components, it has been shown that it is generally sufficient to take the first-order and the second-order reflections into account [20]–[22], [29].

#### B. PDOA-Based Positioning

In this subsection, we briefly introduce the principle of the PDOA algorithm for the multi-cell integrated VLCP system. As discussed in [3], [19], [20], each cell consists of at least three LED lamps which are used in the 2-dimensional (2D) PDOA algorithm with the selected different subcarriers for positioning, where each positioning signal with its positioning frequency on the subcarrier is modulated on its corresponding LED lamp (each positioning frequency occupies one subcarrier). In the PDOA based VLP algorithm we adopted, these signals are modulated on the lightwave carrier with intensity modulation [3], [19], [20]. The phase differences we measure are the sinewave signal (intensity envelope of a few MHz) modulated on the lightwave instead of the phase of the lightwave itself. Hence, PDOA is feasible to realize the positioning function of our system model.

All the LED lamps are synchronized. Hence, the LED lamps can be distinguished by their respective frequencies. Let  $s_{c,i}^{\rm po}$  denotes the modulated positioning signal in cell c. The sinusoidal positioning signals are modulated into the four LED lamps on the four frequencies in the c-th cell, which can be written as

$$\begin{cases}
\operatorname{Cell} 1: s_{1,1}^{\text{po}} = \sin(2\pi f_{i}t), \dots, s_{1,4}^{\text{po}} = \sin(2\pi f_{i+3}t) \\
\operatorname{Cell} 2: s_{2,1}^{\text{po}} = \sin(2\pi f_{i+4}t), \dots, s_{2,4}^{\text{po}} = \sin(2\pi f_{i+7}t) \\
\operatorname{Cell} 3: s_{3,1}^{\text{po}} = \sin(2\pi f_{i+8}t), \dots, s_{3,4}^{\text{po}} = \sin(2\pi f_{i+11}t) \\
\operatorname{Cell} 4: s_{4,1}^{\text{po}} = \sin(2\pi f_{i+12}t), \dots, s_{4,4}^{\text{po}} = \sin(2\pi f_{i+15}t)
\end{cases}$$
(5)

In each cell, at the transmitters, the generated positioning sinusoidal signal are modulated into the four LED lamps on their corresponding positioning frequencies. At the receiver, after separating the received signals with four band pass filters (BFPs), signals with different positioning frequencies are distinguished from each other. Local oscillator acts as a local signal source which generates the local signal with frequency predetermined, while the combination of the synchronized cutter and the peak locator is to synchronize the received signal with the local signal. After passing through the low-pass filtering (LPF) before taking the positioning signal processing, the phase difference of the received signals from different LED lamps calculated, then the location of the device can be estimated using the 2D PDOA method (refer to [19], [20] for the more details).

After estimating the location of each device, the root square error (RSE) of the k-th device can be expressed as

$$RSE_k = \sqrt{(x_{k,e} - x_k)^2 + (y_{k,e} - y_k)^2}$$
 (6)

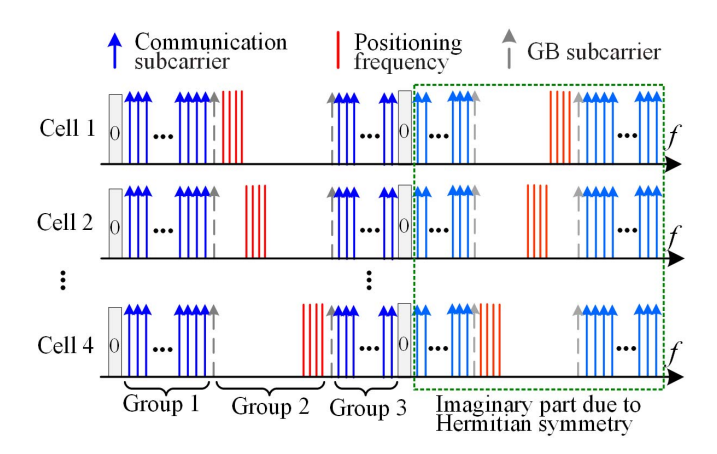


Fig. 2. Subcarrier multiplexing for communication and positioning in the four-cell integrated VLCP system.

where  $\Theta_k^e = (x_{k,e}, y_{k,e})$  and  $\Theta_k = (x_k, y_k)$  are the estimated location and the real location of the k-th device, respectively.

In the integrated VLCP system, the total subcarriers are divided into three groups and several GBs, as shown in Fig. 2, where group 2 (red lines) is used for VLP and the remaining two groups are reserved for VLC. The subcarriers used for positioning of all cells are in the group 2. Generally speaking, subcarriers for positioning can be allocated separately or allocated together. However, when subcarriers for positioning are allocated separately, the system needs more GBs to avoid OOBI between adjacent subbands, so more bandwidth are required to be GBs which will reduce the overall spectral efficiency of the integrated system. By contract, when subcarriers for positioning are allocated together, the system can require only two GBs between adjacent subbands, which can avoid using more GBs compared with the design by allocating positioning subcarriers separately. In this case, we set that subcarriers for positioning are allocated together.

#### C. FBMC/OFDM-Based Subcarrier Multiplexing

In the integrated VLCP system, there are two modulation schemes, OFDM and FBMC. In this subsection, we describe the principle of FBMC and compare it with the widely used OFDM, and apply these two modulation schemes based SCM for the integrated VLCP system.

In order to suppress the large OOBI, FBMC uses a prototype filter to filter each subcarrier. The basic structures of the two modulation schemes are the same, except the cyclic prefix (CP) insertion in OFDM is replaced by the polyphaser network (PPN) based on the well-designed prototype filter [31] in FBMC. Before performing the inverse fast Fourier transform (IFFT) design, Hermitian symmetry is imposed to generate a real-valued signal. The goal of employing PPN in FBMC is to guarantee that FBMC has the same FFT size and similar complexity with those of OFDM. Even though FBMC could significantly reduce the sidelobes through filtering each subcarrier, it may break the pulse-shape orthogonality between adjacent subcarriers. Hence, the off-set quadrature amplitude modulation (OQAM) modulation is applied to guarantee the orthogonality [31]. For OFDM,

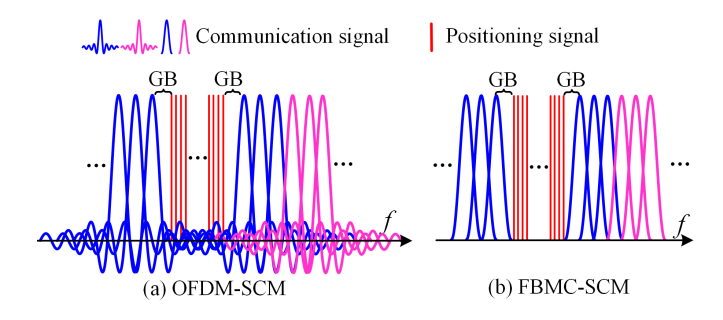


Fig. 3. Illustration of the spectra of (a) OFDM-SCM signal and (b) FBMC-SCM signal in the multi-cell integrated VLCP system.

it applies a low-pass linear phase finite impulse response (FIR) filter to filter the input data, called the Sinc-filter [26], while FBMC uses the Mirabbasi-Martin filter (MM-filter) to filter each subcarrier [31]. It is worth noticing that filtering each subcarrier may break the pulse-shape orthogonality between adjacent subcarriers. Hence, the offset quadrature amplitude modulation (OQAM) modulation is applied to guarantee the orthogonality [31].

The spectra of the communication and positioning signals of the integrated VLCP system based on the mentioned two modulation schemes are depicted in Fig. 3. Compared with OFDM, the OOBI of FBMC spectrum is effectively suppressed, which has low interference leakage to adjacent subcarriers. For OFDM, the high OOBI results in severe interference among adjacent subcarriers, leading to decrease the positioning accuracy and communication performance.

At the receiver, for the communication signal, the received SINR can be defined as the desired received electronic communication power over the noise power plus the sum of the received interference from other cells' transmitters and the OOBI. Then, when the k-th device is served by the c-th cell, its received signal-to-interference-plus-noise-ratio (SINR) on the n-th subcarrier can be given by

$$\gamma_{k,c,n}^{\text{co}} = \frac{\mu^2 \sum_{m \in \mathcal{M}_c} P_{m,c,n}^{\text{co}} (h_{k,m,c}^n)^2}{\mu^2 \sum_{c' \neq c} \sum_{m \in \mathcal{M}_{c'}} P_{m,c',n}^{\text{co}} (h_{k,m,c'}^n)^2 + I_{c,n}^{\text{oobi}} + \delta^2}$$
(7)

where  $\mu$  denotes the PD's responsivity.  $h^n_{k,m,c}$  represents the channel gain on the n-th subcarrier from the m-th LED lamp to the k-th device in cell c.  $I^{\rm cobi}_{c,n}$  shows the OOBI on the n-th communication subcarrier from adjacent subcarriers' communication signal in cell c. In (7), we can observe that the received signal may suffer ICI and OOBI from other cells when the device locates in the overlapped area. Otherwise, it cannot suffer ICI or OOBI from other cells and these two types of interference are not considered in (7).

For the k-th device, the achievable rate on the n-th subcarrier in cell c can be expressed as

$$R_{k,c,n} = \frac{B_{sub}}{2} \log_2(1 + \gamma_{k,c,n}^{co})$$
 (8)

where  $B_{sub}$  is the subcarrier bandwidth  $B_{sub} = B/N$  with B being the system transmission bandwidth, and the scaling factor 1/2 is due to the Hermitian symmetry [23], [26].

## III. SYSTEM CONSTRAINTS AND PROBLEM FORMULATION

In this section, we formulate a theoretical optimization problem for the coordinated resource allocation in the multicell integrated VLCP system with the objective of maximizing the sum rate of IoT devices while guaranteeing the practical constraints related to both VLC and VLP scenarios.

## A. VLCP System Constraints

In practical integrated VLCP systems, some certain constraints should be considered in the optimization problem, which are discussed and analyzed as follows:

1) Power Constraint: Differing from the RF systems, three unique issues for power allocation must be taken account into VLCP systems due to the inherent characteristics of white LEDs based VLCP systems: (1) the transmitted signals must be non-negative; (2) the optical power should be operated in the limited linear optical power range due to the non-linearity of LEDs and the maximum permissible optical intensity for the sake of eye safety [5], [10], [29]; (3) the illumination (brightness levels) requirement in the room. As analyzed above, the transmitted signal at each LED lamp should satisfy [5], [10], [29]

$$A_{\min} \le z_{c,m} \le A_{\max} \tag{9}$$

where  $A_{\min}$  and  $A_{\max}$  denote the minimum and maximum values of each LED lamp' driving current in the region of  $[A_{\min}, A_{\max}]$ , which should satisfy the above three mentioned inherent characteristics of white LEDs.

Then, combining (1) and (9), we can get the constraint on the allocated electrical power at each LED lamp in each cell, which is given by

$$\frac{A_{\min} - A}{\sigma} \leq \sum_{k \in \mathcal{K}} \sum_{n \in \mathcal{N}_{c,co}} \rho_{k,c,n}^{\text{co}} \sqrt{P_{m,c,n}^{\text{co}}} + \sqrt{P_{m,c,i}^{\text{po}}} \\
\leq \frac{A_{\max} - A}{\sigma} \tag{10}$$

In addition to the constraint in (10), at each LED lamp in the c-th cell, the transmit electrical power allocated to the associated devices across all subcarriers should be less than the maximum transmit electrical power of each LED lamp, which can be expressed as

$$\sum_{k \in \mathcal{K}} \sum_{n \in \mathcal{N}_{c,co}} \rho_{k,c,n}^{\text{co}} P_{m,c,n}^{\text{co}} + P_{m,c,i}^{\text{po}} \le P_{\text{max}}$$
 (11)

2) QoS Constraints of VLC: One of the key purposes of the VLCP system is to provide the communication services for the devices, so the minimum transmission data rate of these devices must be satisfied in the performance optimization design. Thus, the resulting constraint is expressed by

$$R_k = \sum_{n \in \mathcal{N}_{c,co}} \rho_{k,c,n}^{\text{co}} R_{k,c,n} \ge R_k^{\text{min}}$$
 (12)

where  $R_k^{\min}$  is the minimum data rate requirement of the k-th device.

3) Positioning Accuracy Constraints of VLP: In addition to the QoS constraint in (12) of VLC, VLCP systems should guarantee that the positioning accuracy requirement of the devices, in other words, the k-th device' current positioning error must be below its given positioning error threshold  $RSE_{k}^{\max}$ .

Without loss of generality, when other parameters are fixed, the positioning error (RSE) can be expressed as an explicit function of transmit electrical power levels by using the Cramer-Rao Lower Bound (CRLB) [32]. At each receiver, the 2D positioning uses at least three received positioning signal to perform devices' location estimation. Then, we suppose that the k-th device employs i = 1, 2 and 3 positioning subcarriers to perform positioning, the CRLB on the PDOA algorithm is given by [32]

$$RSE_{k}^{CRLB} \approx \max \left[ \sum_{i=1}^{2} \frac{c^{2}}{(2\pi\sqrt{3}f_{c})t_{s}\sqrt{3}f_{c}(P_{i}^{po}h_{k,i}^{2}\mu^{2})/\delta^{2}} , \right.$$

$$\left. \sum_{i=2}^{3} \frac{c^{2}}{(2\pi\sqrt{3}f_{c})t_{s}\sqrt{3}f_{c}(P_{i}^{po}h_{k,i}^{2}\mu^{2})/\delta^{2}} \right]^{1/2}$$
(13)

where  $f_{\rm c}$  is the carrier frequency. Hence, we have the constraint

$$RSE_k^{CRLB} \le RSE_k^{max}$$
 (14)

#### B. Problem Formulation

In the multi-cell integrated VLCP system, the objective of our proposed coordinated resource allocation approach is to globally maximize the sum rate of devices, while considering the above mentioned constraints in Section III.B. The problem of the coordinated resource allocation for multi-cell integrated VLCP systems can be mathematically formulated as follows

$$\underset{\boldsymbol{\rho}_{\text{co}}, \, \mathbf{P}_{\text{co}}, \, \mathbf{P}_{\text{po}}}{\text{maximize}} \sum_{c \in \mathcal{C}} \sum_{k \in \mathcal{K}} \sum_{n \in \mathcal{N}_{c, \text{co}}} \rho_{k, c, n}^{\text{co}} R_{k, c, n} \qquad (15a)$$

$$s.t. (10); (11); (12); (14);$$
 (15b)

$$\rho_{k,c,n}^{\text{co}} \in \{0,1\}, \quad \forall c, k, n;$$
 (15c)

$$\rho_{k,c,n}^{\text{co}} \in \{0,1\}, \quad \forall c, k, n;$$

$$\sum_{k \in \mathcal{K}} \sum_{n \in \mathcal{N}_{c,co}} \rho_{k,c,n}^{\text{co}} \leq N_{c,co}, \quad \forall c.$$
(15d)

where  $\rho_{co}$  denotes the vector of subcarrier allocation variables for communication and positioning.  $\mathbf{P}_{\text{co}} = [\mathbf{P}_1^{\text{co}}, \dots, \mathbf{P}_C^{\text{co}}]^T$ is the set of transmit electrical power allocation matrices for communication, where  $\mathbf{P}_c^{\text{co}} = [P_{c,1}^{\text{co}}, P_{c,2}^{\text{co}}, \dots, P_{c,N_{c,co}}^{\text{co}}]^T$ . In (15), (15d) is used to ensure that the sum of assembled subcarriers for communication should not exceed the number of the available communication subcarriers in each cell.

Clearly, the optimization problem in (15) is a mixed-integer programing problem due to the binary variables  $ho_{co}$ , as well as the non-negative variables  $P_{\rm co}$  and  $P_{\rm po}$  are involved. In addition, the optimization problem for maximizing (14a), given constraints in (10)-(12), (14), (15c), (15d), is also a NP-hard problem, so that it cannot be solved directly. Hence, in the following section, we show how to effectively solve the optimization problem in (15) in the coordinated multi-cell integrated VLCP system.

# IV. SOLUTION OF THE COORDINATED RESOURCE ALLOCATION PROBLEM

As analysis at the end of the previous section, it is quite difficult to solve the optimization problem in (15) to obtain the optimum in the coordinated formulation. Hence, in this section, we solve the joint optimization problem in (15) by decomposing it into two subproblems: a subcarrier allocation problem and a power allocation problem. Consequently, after solving these two subproblems alternately, we can achieve the optimized solution of the joint optimization problem in (15) by using an iterative algorithm.

## A. Suboptimal Subcarrier Allocation

In this subsection, we show how to achieve the communication subcarrier allocation when the power allocation is given. We can observe that the optimization problem in (15) is a combinatorial problem in terms of subcarrier allocation, which has a prohibitive computational complexity if we solve it through using the exhaustive search for all the possible cases, especially when the number of devices and subcarriers are large in the integrated VLCP system. Hence, we propose a low-complexity approach to achieve the suboptimal subcarrier allocation under the devices' minimum data rate requirements.

Firstly, for the k-th device, we define the channelto-interference-and-noise radio on the n-th communication subcarrier as,

$$G_{k,c,n}^{\text{co}} = (I_{c,n}^{\text{ICI}} + I_{c,n}^{\text{oobi}} + \delta^2)^{-1}$$
 (16)

where  $I_{c,n}^{\rm ICI}$  denotes the ICI from adjacent cells on the n-th subcarrier in cell c.

The main principle of the proposed suboptimal subcarrier allocation approach is based on the above mentioned channel quality information in (16), which can be presented by the following analysis. Firstly, we search the device whose current rate is the farthest away from its target minimum rate requirement and set that the device has the priority to be allocated the high-quality subcarriers (high channel-tointerference-and-noise) to meet its QoS requirement. After guaranteeing the QoS requirements of all devices, we allocate the excess communication subcarriers to maximize the global sum rate of devices. It is important to note that the goal of the above subcarrier allocation mechanism is to satisfy the constraint (12) of the optimization problem in (15) before maximizing the objective function in (15a), which is different from the existing classical approaches that maximize the system sum rate without considering the constraints in their optimization problem.

The algorithm of the suboptimal subcarrier allocation is shown in Algorithm 1. Let G denote the channel-tointerference-and-noise channel quality matrix.

The optimal subcarrier allocation can be achieved if we adopt the exhaustive search for all the possible subcarrier allocation cases. In our multi-cell integrated VLCP system with the K-device and N-subcarrier per cell, it is prohibitive to search the optimum due to the high computational complexity, since the exhaustive search scheme has  $C \times K^{N_{\text{co}}}$  possible subcarrier allocations, especially the complexity is quite big

# Algorithm 1 Suboptimal Subcarrier Allocation

1: Initialization:  $\mathcal{N}_{c,\text{co}} = \{1,\ldots,\overline{N_{c,\text{co}}}\}, \mathcal{K} = \{1,\ldots,K\}$ for c = 1, ..., C, channel quality matrix G, set  $R_k = 0$  and  $\Omega_k = \emptyset$  for  $\forall k \in \mathcal{K}$ ;

Step 1: Allocate communication subcarriers to satisfy devices' minimum rate requirements

2: For c = 1 to C do

3: For any device k satisfying  $R_k < R_k^{\text{tar}}$ ;

4: Find the device k' satisfying  $R_k^{\text{tar}} - R_k \leq R_{k'}^{\text{tar}} - R_{k'}$  for  $\forall k' \in \mathcal{K};$ 

5: For k' in cell c, find n' satisfying  $G_{k',c,n'}^{co} \geq G_{k',c,n}^{co}$  for

6: For k' and n' in cell c, let  $\Omega_{k'} = \Omega_{k'} \cup \{n'\}, \mathcal{N}_{c,co} =$  $\mathcal{N}_{c,co} - \{n'\}$ , and update  $R_{k'}$ ;

7: **End** 

Step 2: Allocate remaining subcarriers to maximize the system sum rate

8: For c=1 to C do

9: While  $N_{c,co} \neq \emptyset$ 

10: In cell c, find the device k' satisfying  $\sum_{m \in \mathcal{M}_c} (h_{k',m,c})^2 \ge \sum_{m \in \mathcal{M}_c} (h_{k,m,c})^2 \text{ for } \forall k' \in \mathcal{K};$ 11: For k', find n' satisfying  $G_{k',c,n'}^{\text{co}} \ge G_{k',c,n}^{\text{co}}$  for

For k' and n' in cell c, let  $\Omega_{k',c} = \Omega_{k',c} \cup \{n'\},\$  $\mathcal{N}_{c,co} = \mathcal{N}_{c,co} - \{n'\}, \text{ and update } R_{k'}.$ 

13: **End** 

14: **End** 

when the number of devices and subcarriers are large in the system. However, the complexity of our proposed suboptimal subcarrier allocation is  $C \times K \times N_{co}$ , which is great lower than that of the exhaustive search method.

# B. Power Allocation With Given Subcarrier Allocation

After allocating the subcarrier according to **Algorithm 1**, here, we present an optimal power allocation approach with given suboptimal subcarrier allocation  $\rho_{co}$ . The problem in (15) is reduced to the sum rate maximization with respect to the communication power allocation  $P_{\rm co}$  and positioning power allocation  $P_{po}$  while maintaining the constraints (10)-(12), (14), (15c) and (15d). Hence, the problem in (15) is formulated with the following form.

maximize 
$$\sum_{\mathbf{P}_{co}, \mathbf{P}_{po}} \sum_{c \in \mathcal{C}} \sum_{k \in \mathcal{K}} \sum_{n \in \mathcal{N}_{c,co}} \rho_{k,c,n}^{co} R_{k,c,n}$$
  
s.t. (9); (10); (11); (13); (14c); (14d). (17)

Clearly, the power allocation problem in (17) is a non-convex and non-linear programming problem in  $P_{co}$  and  $P_{DO}$ , which makes the global optimal solution intractable. In order to solve it, we use the Sequential Quadratic Programming (SQP) method [33] to obtain the global optimal solution  $P_{co}$  and  $P_{po}$ , which is capable of solving the non-linearly constrained optimization problems [33]. Due to the non-linear constraints (10)-(12) and (14), the SQP method is an effective approach to solve our formulated optimization problem in (17)

by converting it into the choice of quadratic sub-problems with a quadratic objective function.

The Lagrangian function of the optimization problem in (17) can be expressed as

$$\mathcal{L}(\mathbf{P}_{co}, \mathbf{P}_{po}, \boldsymbol{\lambda}) = \sum_{c \in \mathcal{C}} \sum_{k \in \mathcal{K}} \sum_{n \in \mathcal{N}_{c,co}} \rho_{k,c,n}^{co} R_{k,c,n} 
+ \sum_{c \in \mathcal{C}} \sum_{m \in \mathcal{M}_{c}} \lambda_{m,c}^{c1} \alpha_{m,c}(\mathbf{P}) + \sum_{c \in \mathcal{C}} \sum_{m \in \mathcal{M}_{c}} \lambda_{m,c}^{c2} \beta_{m,c}(\mathbf{P}) 
+ \sum_{c \in \mathcal{C}} \sum_{m \in \mathcal{M}_{c}} \lambda_{m,c}^{c3} \mu_{m,c}(\mathbf{P}) + \sum_{c \in \mathcal{C}} \sum_{k \in \mathcal{K}} \lambda_{k,c}^{c4} \nu_{k,c}(\mathbf{P}) 
+ \sum_{c \in \mathcal{C}} \sum_{k \in \mathcal{K}} \lambda_{k,c,i}^{c5} \omega_{k,c,i}(\mathbf{P})$$
(18)

where 
$$\alpha_{m,c}(\mathbf{P}) = \sum_{k \in \mathcal{K}} \sum_{n \in \mathcal{N}_{c,co}} \rho_{k,c,n}^{\text{co}} \sqrt{P_{m,c,n}^{\text{co}}} + \sqrt{P_{m,c,i}^{\text{po}}} - \frac{A_{\min} - A}{\sigma};$$

$$\beta_{m,c}(\mathbf{P}) = \frac{A_{\max} - A}{\sigma} - \sum_{k \in \mathcal{K}} \sum_{n \in \mathcal{N}_{c,co}} \rho_{k,c,n}^{\text{co}} \sqrt{P_{m,c,n}^{\text{co}}} - \sqrt{P_{m,c,i}^{\text{po}}};$$

$$\mu_{m,c}(\mathbf{P}) = P_{\max} - \sum_{k \in \mathcal{K}} \sum_{n \in \mathcal{N}_{c,co}} \rho_{k,c,n}^{\text{co}} P_{m,c,n}^{\text{co}} + P_{m,c,i}^{\text{po}};$$

$$\nu_{k}(\mathbf{P}) = \sum_{n \in \mathcal{N}_{c,co}} \rho_{k,c,n}^{\text{co}} R_{k,c,n} - R_{k}^{\min};$$

$$\omega_{k}(\mathbf{P}) = RSE_{k}^{\max} - RSE_{k}^{\text{CRLB}}.$$
where  $\lambda = (\lambda^{c1}, \lambda^{c2}, \lambda^{c3}, \lambda^{c4}, \lambda^{c5})$ , which is the dual Lagrange variable matrix for the constraints (11)-(12)

where

dual Lagrange variable matrix for the constraints (11)-(12)

The SQP method needs a finite number of iterations to converge the optimal point of the optimization problem in (17), and the t-th iteration of the function (18) is formulated by a quadratic programming sub-problem with an approximate solution  $\mathbf{P}(t) = [\mathbf{P}_{co}(t) \ \mathbf{P}_{po}(t)]$ . And the initial approximation solution is  $\mathbf{P}(0) = [\mathbf{P}_{co}(0) \ \mathbf{P}_{po}(0)]$ . In order to solve the formulated problem in the SQP format, we define the SQP vector of the constraints (10)-(12) and (14) as

$$\mathbf{F}(\mathbf{P}) = [\alpha(\mathbf{P}), \beta(\mathbf{P}), \mu(\mathbf{P}), \nu(\mathbf{P}), \omega(\mathbf{P})]$$
(19)

where  $\alpha(\mathbf{P}) = [\alpha_1(\mathbf{P}), \dots, \alpha_C(\mathbf{P})]^T$ ,  $\beta(\mathbf{P}) = [\beta_1(\mathbf{P}), \dots, \beta_C(\mathbf{P})]^T$ ,  $\mu(\mathbf{P}) = [\mu_1(\mathbf{P}), \dots, \mu_C(\mathbf{P})]^T$ ,  $[\nu_1(\mathbf{P}), \dots, \nu_K(\mathbf{P})]^T$  and  $\omega(\mathbf{P})$  $\nu(\mathbf{P}) =$  $[\omega_1(\mathbf{P}), \dots, \omega_K(\mathbf{P})]^T$  are the SQP format maxtrix.

To solve the problem in (18), at each iteration t, the SQP method improves the estimate solution  $(\mathbf{P}(t), \mathbf{F}(t))$  with a correction vector  $\mathbf{s}(t) = [\mathbf{s}_{\mathbf{p}}^T(t) \ \mathbf{s}_{\mathbf{r}}^T(t)]^T$ . The correction vector is achieved by solving the following quadratic programming problem

$$\min \frac{1}{2} \langle \mathbf{s}, \nabla^2 [\mathcal{L}(\mathbf{P})] \mathbf{s} \rangle + \langle \nabla [\mathcal{L}(\mathbf{P})], \mathbf{s} \rangle$$
 (20a)  

$$s.t. \ \nabla [\mathbf{F}(\mathbf{P})] \mathbf{s} + \mathbf{F}(\mathbf{P}) \mathbf{s} \ge 0.$$
 (20b)

where  $\nabla[\cdot]$  and  $\nabla^2[\cdot]$  are the first-order and second-order partial derivatives, respectively, and  $\nabla^2[\cdot]$  is also the Hessian operator. The SQP method updates the pair of solution  $(\mathbf{P}(t), \mathbf{F}(t))$  at each iteration to minimize the function (20a). In other words, the allocated electrical power and the dual Lagrange variables are estimated by finding the correction

# Algorithm 2 Coordinated Resource Allocation for Multi-Cell Integrated VLCP Systems

1: **Initialization:** Set the iteration j = 0, initialize  $\rho_{co(0)}$  and P(0), the maximum tolerance  $\varsigma > 0$ . The central controller collects devices' information, and shares the information among cells;

# 2: Repeat

- 3: Update the communication subcarrier allocation  $\rho_{co}(j+1)$ in **Algorithm 1** with given P(0);
- Update the communication and positioning power allocation P(j + 1) by solving (14) using the SQL method with given  $\rho_{co}(j+1)$ ;
- 5: Update  $j \leftarrow j + 1$ ;

6: Calculate 
$$R_{\text{total}}(\boldsymbol{\rho}_{\text{co}}(j), \mathbf{P}(j)) = \sum_{c \in \mathcal{C}} \sum_{k \in \mathcal{K}} \sum_{n \in \mathcal{N}_{c,\text{co}}} \rho_{k,c,n}^{\text{co}} R_{k,c,n};$$
7: Until  $|R_{\text{total}}(\boldsymbol{\rho}_{\text{co}}(j), \mathbf{P}(j)) - R_{\text{total}}(\boldsymbol{\rho}_{\text{co}}(j-1), \mathbf{P}(j-1))|$ 

- $1))| \leq \varsigma;$
- 8: **End**
- 9: Output:  $\rho_{co}^* \leftarrow \rho_{co}(j)$ , and  $\mathbf{P}^* \leftarrow \mathbf{P}(j)$ .

vector  $\mathbf{s}(t)$  at the t-th iteration, which are expressed as follows

$$\begin{bmatrix} \nabla^{2}[\mathcal{L}(\mathbf{P}(t))] & \nabla[\mathbf{F}(\mathbf{P}(t))]^{T} \\ \nabla[\mathbf{F}(\mathbf{P}(t))] & \mathbf{0} \end{bmatrix} \times \begin{bmatrix} \mathbf{s}_{\mathbf{P}}(t) \\ -\mathbf{s}_{\mathbf{F}}(t) \end{bmatrix}$$
$$= -[\nabla[\mathcal{L}(\mathbf{P}(t))] \mathbf{F}(\mathbf{P}(t))]^{T} \quad (21)$$

In (21), the Karush-Kuhn-Tucker (KKT) condition is used to solve the SQP quadratic problem in (20) by taking  $\nabla [\mathbf{F}(\mathbf{P}(t))]\mathbf{s} + \mathbf{F}(\mathbf{P}(t)) = 0$ , hence the set of constraints (10)-(12) and (14) are active constraints at each iteration [33]. At each iteration, the SQP method provides a better estimated solution towards to the optimal solution point when the convergence is guaranteed within a finite number of iterations [33]. In addition, the step size parameters  $\varepsilon_{\mathbf{P}}(t)$  and  $\varepsilon_{\mathbf{F}}(t)$  are chosen by applying a merit function  $\Phi(\cdot)$  [33], and the step size is selected to reduce the value of the merit function. The process is measured by the merit function  $\Phi(\cdot)$ , and when  $\Phi(\cdot)$  is maximized by the selection of the step size  $\varepsilon_{\mathbf{P}}(t)$ , that is,  $\Phi(\mathbf{P}(t) + \beta_{\mathbf{P}}(t)\mathbf{s}_{\mathbf{P}}(t))$  is sufficiently small. The step sizes  $\varepsilon_{\mathbf{P}}(t)$  and  $\varepsilon_{\mathbf{F}}(t)$  are usually set to 1 [33]. In addition, the interior point scheme is adopted in the SQP programing, the solution details can be found in [33].

Finally, according to (18)-(21), we can achieve the optimal power allocation in the coordinated multi-cell integrated VLCP system by applying the SQP method.

# C. Coordinated Resource Allocation in Multi-Cell Integrated VLCP Systems

Accordingly, we present the solution process for the coordinated resource allocation in the multi-cell integrated VLCP system, as shown in **Algorithm 2**. The algorithm iteratively updates the subcarrier allocation and the transmit electrical power, in order to coverage the optimized solution point.

Here, we analyze the computational complexity of Algorithm 2. As analyzed in Section IV.B, updating the

TABLE I SIMULATION PARAMETERS

Parameters	Values
Room size (length × width × height )	10×10×3 m <sup>3</sup>
Number of cells	4
Number of LED lamps per cell	4
Number of PDs per user	1
User height	0.85
Transmitter semi-angle	60°
Lambertian emission order	1
Positioning error threshold	7.5 cm
Noise power spectral density	$10^{-20}A^2/Hz$
PD concentrator index	1.5
PD area	$0.5 \text{ cm}^2$
Gain of optical filter	1.0
PD responsivity	0.5 A/W
FOV of the PD	120°
Minimum rate requirement	10 Mbit/s
Transmission bandwidth	40 MHz
IFFT/FFT size	256
Overlapping factor of FBMC	4

TABLE II LOCATIONS OF LED LAMPS IN EACH CELL

Cell index	Locations of three LED lamps in each cell (unit: m)
Cell 1	[-2, 2, 3], [-3, 2, 3], [-2, 3, 3], [-3, 3, 3]
Cell 2	[2, 2, 3], [3, 2, 3], [2, 3, 3], [3, 3, 3]
Cell 3	[-2, -2, 3], [-3, -2, 3], [-2, -3, 3], [-3, -3, 3]
Cell 4	[2, -2, 3], [3, -2, 3], [2, -3, 3], [3, -3, 3]

subcarrier allocation needs the complexity of  $C \times K \times N_{co}$ . In addition, the complexity of updating the power allocation is  $O(CM(N)^3 \log(1/\zeta))$ . Then, the overall computational complexity of Algorithm 2 is  $O(CM(N)^3 \log(1/\zeta) + C \times$  $K \times N_{\rm co}$ ).

# V. Numerical Results and Discussion

In this section, we evaluate the performance of the presented multi-cell integrated VLCP system based on two modulation schemes (namely, FBMC-SCM and OFDM-SCM), as well as provide the numerical results to verify the effectiveness of our proposed resource allocation approach by comparing it with other approaches.

We consider an indoor four-cell integrated VLCP in a room of size of  $10 \times 10 \times 3$  m<sup>3</sup> with a number of IoT device being randomly located on the floor in the room, where each cell has four LED lamps and each device is equipped with a single PD. The positioning error threshold of each device is 7.5 cm, and the minimum data rate requirements of each device is 10 Mbit/s. The system parameters and locations of LED lamps are listed in Table I and Table II, respectively. Other relevant parameters can be seen in [13]. In the indoor environment, the typical reflection coefficients of 0.3 for the floor and 0.8 for the walls and ceiling were used for room.

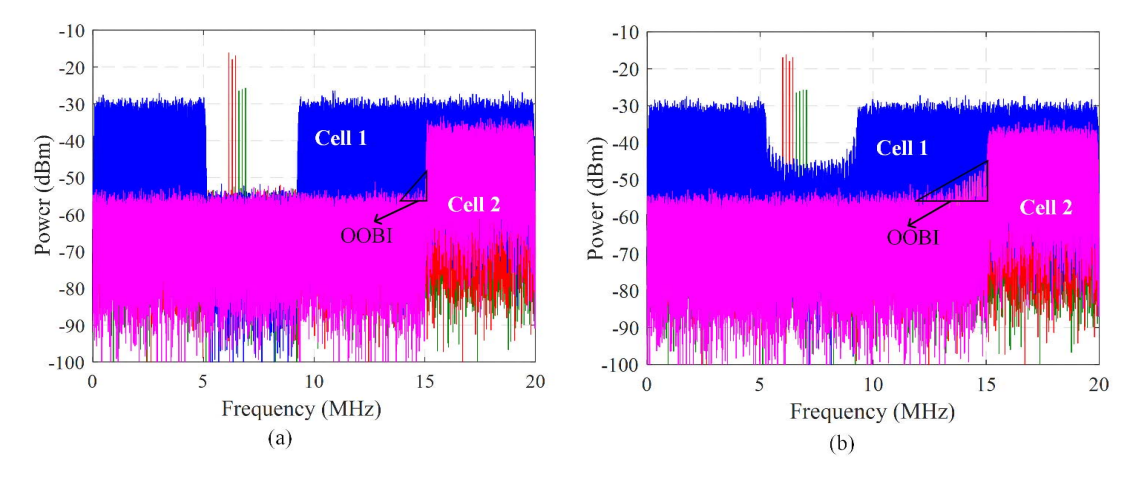


Fig. 4. Spectra of (a) FBMC-SCM signal and (b) OFDM-SCM signal in the multi-cell integrated VLCP system. Note: com., spe., and pos. denote communication, spectra and positioning, respectively.

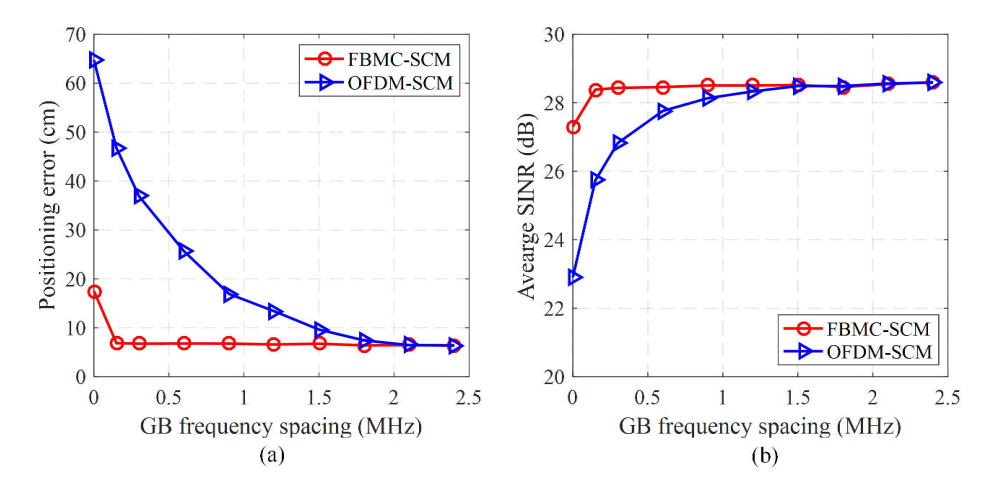


Fig. 5. Comparisons of (a) average positioning error and (b) average SINR performance versus each GB frequency spacing in the multi-cell integrated VLCP system.

We run the simulation 100 times with random device locations and obtain the average statistics.

Note that the frequency range used for positioning (16 positioning subcarriers) is from 6.0 MHz to 8.4 MHz in the four-cell integrated VLCP system with each frequency gap of about 0.15 MHz [19], [27]. We use this range of frequency for positioning for the following reasons. The frequency is inversely proportional to a phase resolution, it is directly related to the positioning error [19], [27]. On one hand, if the positioning frequencies are selected at the low frequency region, the location errors are increased due to low phase resolution. On the other hand, even though high positioning frequency for positioning can achieve good phase resolution, the severe power attenuation of the high frequency components will reduce the positioning accuracy performance [19], [27]. Hence, as a trade-off between phase resolution and power attenuation, we use this range of frequency for positioning.

# A. Comparisons of FBMC-SCM and OFDM-SCM Based Multi-Cell Integrated VLCP Systems

Fig. 4(a) and (b) plot the spectra of both the received FBMC-SCM signal and OFDM-SCM signal, respectively,

where the GB spacing between the communication subcarriers and positioning subcarriers is 0.9 MHz and the device locates at [-0.5m, 2.5m, 0.85m]. Note: the device associates with cell 1 and locates in the overlapped area where it only receives interference from cell 2, and we take one case as an example to analyze the system performance in Fig. 5.

For positioning subcarriers, no matter where the device locate (the overlapped or non-overlapped area), it suffers the serious OOBI if the system uses OFDM-SCM, while a great 9-dB OOBI reduction can be obtained by using FBMC-SCM compared with OFDM-SCM. For communication subcarriers, the devices only locate in the overlapped areas may suffer the OOBI from adjacent cells by using OFDM-SCM. We can see observe that compared with OFDM, the OOBI of FBMC is effectively suppressed, leading to much reduced OOBI leakage on the positioning subcarriers and communication subcarriers, thus avoid the positioning accuracy and communication performance degradation.

Figs. 5(a) and (b) show the average positioning errors and the average received communication SINR versus the GB frequency spacing, respectively. As can be seen from the figures, both the positioning accuracy and the SINR value of FBMC-SCM outperform that of OFDM-SCM in the

multi-cell integrated VLCP system when the GB spacing is small. FBMC-SCM does not need the large GB spacing to mitigate the OOBI. However, the positioning accuracy and the SINR performance are much sensitive to the GB spacing in OFDM-SCM. It can further be seen that OFDM-SCM achieves nearly the same positioning accuracy and SINR performance as the FBMC-SCM only when the GB spacing are about 2.1 MHz and 1.5 MHz, respectively. Since the positioning accuracy and the SINR of FBMC-SCM become stable when the GB spacing is about 0.15 MHz, much smaller GB pacing is required by using FBMC-SCM. By defining the effective subcarrier utilization ratio (ESUR) as the ratio of the effective subcarriers occupied by the subcarriers for communication and positioning to the total subcarriers, FBMC-SCM improves the ESUR from 79% to 97% compared with OFDM-SCM when the two modulation schemes has the same positioning performance.

## B. Comparisons of Different Resource Allocation Approaches

In this subsection, we compare the performance of different resource allocation approaches in the multi-cell integrated VCLP system based on FBMC-SCM when the GB spacing is 0.15 MHz, these approaches are:

- Coordinated optimal resource allocation approach (denoted as coordinated optimal RA): The system uses the exhaustive search method to find the optimal subcarrier allocation strategy.
- Coordinated resource allocation (denoted as coordinated RA): The joint subcarrier and power allocation approach with the purpose of guaranteeing the global practical constraints while maximizing the global sum rate of devices under cell coordination.
- Coordinated power allocation with equal subcarrier allocation (denoted as coordinated PA-ESA): The power allocation is adopted by Section III.C under cell coordination and the communication subcarriers are equally allocated to devices.
- Coordinated subcarrier allocation with equal power allocation (denoted as coordinated SA-EPA): The subcarrier allocation is adopted by Section III.B under cell coordination and the transmit electrical power is equally allocated to each communication subcarrier and each positioning frequency, i.e.,  $P_{c,1}^{\rm co} = P_{c,2}^{\rm co}, ..., P_{c,N_{\rm co}}^{\rm co}$  and  $P_{c,1}^{\rm po} = P_{c,2}^{\rm po}, ..., P_{c,N_{\rm po}}^{\rm po}$ . Considering the SINR requirements of the PDOA positioning, the transmit electrical power on each positioning frequency is larger than that of each communication subcarrier by 15dB [19], [27].
- Non-coordinated resource allocation (denoted as non-coordinated RA): Each cell selfishly optimizes its joint subcarrier and power allocation strategy to maximize its data rate while guaranteeing the practical constraints in each cell without coordinating with other cells.

Fig. 6 presents the average sum rate of devices per cell versus maximum transmit electrical power  $P_{\rm max}$  per LED lamp when the total number of devices is K=40. In Fig. 6, as the increase of  $P_{\rm max}$ , the communication performance of

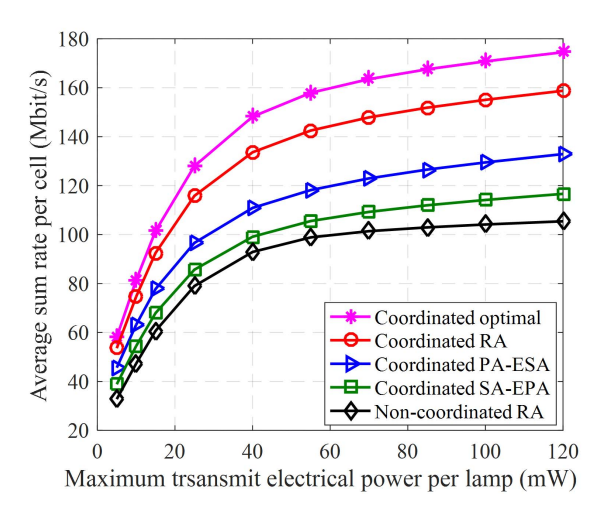


Fig. 6. Average sum rate per cell versus the maximum transmit electrical power per LED lamp.

all approaches improves due to the enhanced received SINR. We can observe that all the coordinated approaches achieve the higher sum rate than that of the non-coordinated RA approach, especially the advantage becomes more significant in the high electrical power regions. This is because the ICI is one of the key factors on the data rate loss as the background noise is no longer dominant in the high electrical power regions, and the interference is proportional to the transmit power, the coordinated approaches effectively remove or minimize the ICI in the multi-cell integrated VLCP system through enabling cell coordination to reduce the total ICI, leading to the performance improvement compared with the uncoordinated RA approach. However, in the uncoordinated RA approach, each cell separately designs the resource allocation, which are multiple single-cell performance optimization problems, hence each cell in its own cell selfishly maximizes its performance without considering the generated ICI to adjacent cells.

In addition, in Fig. 6, the three power allocation approaches outperform the coordinated SA-EPA approach because they are capable of dynamically allocating the transmit electrical power according to the channel gains and the generated ICI, which can effectively improve the sum rate. Moreover, the sum rate of the coordinated RA approach is greater than that of the coordinated PA-ESA approach. In particular, when the QoS requirements are ensured, the system sum rate can be enhanced by allocating remaining subcarriers to the devices who have good channel gains.

Fig. 7 shows the average positioning error performance versus the maximum transmit electrical power  $P_{\rm max}$  per LED lamp when K=40. We can observe that the positioning error of all approaches decreases significantly as the increase of  $P_{\rm max}$  when  $P_{\rm max}$  is less than 70mW, but the performance is appropriately maintained at a horizontal level when  $P_{\rm max}$  exceeds 70mW for the three power allocation approaches. Such the performance improvement results from the high received SINR due to the more transmit power being allocated on positioning subcarriers when  $P_{\rm max}$  is large. Once the positioning accuracy requirements are guaranteed in the high maximum power regions, the extra power will be

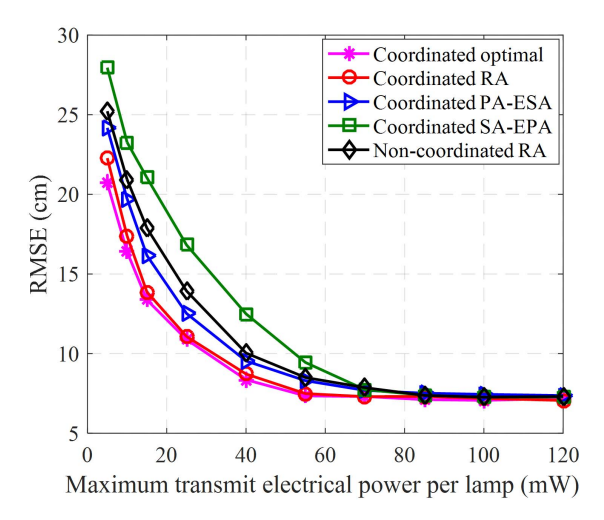


Fig. 7. Average positioning error versus the maximum transmit electrical power per LED lamp.

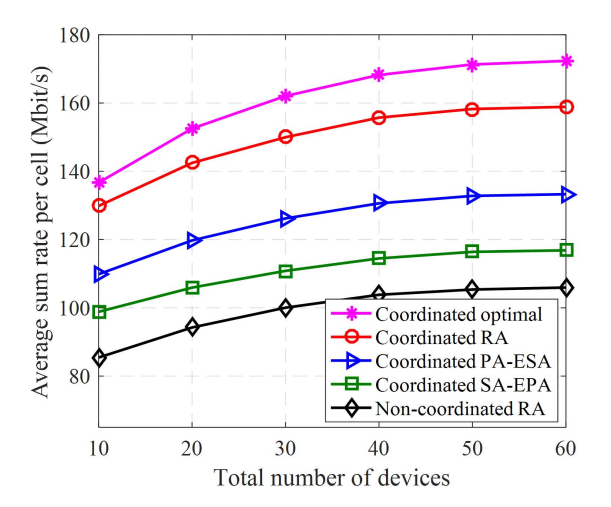


Fig. 8. Average sum rate per cell with varying total number of devices.

allocated to maximize the sum rate of devices as shown in the optimization problem (14), thus the positioning accuracy performance is constant in the high maximum power regions ( $P_{\rm max} > 80 mW$ ). Moreover, we find that the coordinated SA-EPA approach has the worst performance, because the equal power allocation strategy for positioning subcarriers is unreasonable due to the different channel gains from the LED lamps to each device in the device's associated cell.

Fig. 8 shows the average sum rate per cell versus the total different numbers of devices when the maximum transmit electrical power per lamp is 80 mW. We can see that the sum rate per cell of the four approaches improves as the increase number of devices, because the system has the more probability of searching devices having good channel gains to enhance the sum rate of devices for the four approaches, and the coordinated RA approach achieves the best sum rate performance.

Fig. 9 shows the average positioning error performance with varying the total number of devices when the maximum transmit electrical power per lamp is 80 mW. It is interesting

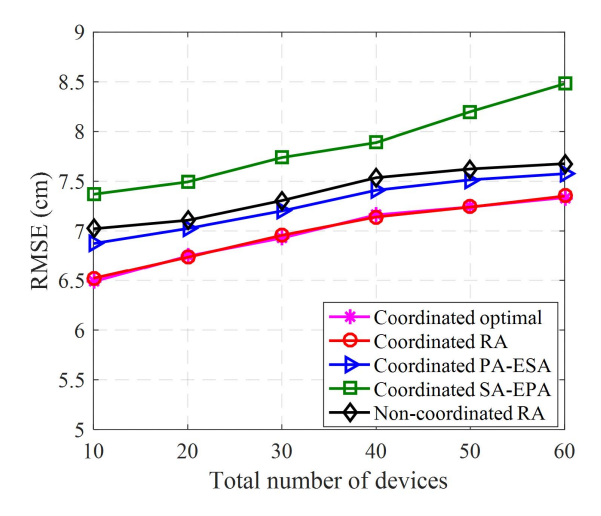


Fig. 9. Average positioning error with varying total number of devices.

to note that the positioning error of the coordinated SA-EPA approach increases as the increase number of devices, while other three approaches almost maintains the positioning error at a horizontal level (may be with a slight increase). The reason can be explained as follows. The larger number of devices leads to the wide range channel gains from different LED lamps to each device in the integrated VLCP system, hence the equal power allocation strategy of the coordinated SA-EPA approach fails to allocate the power on the positioning subcarriers at different LED lamps in each cell under the complex channel gains' environment, while other three approaches has the ability to adjust their power allocation strategy to optimize the positioning accuracy performance in the presence of the complex environment.

## C. Performance Evaluations Under Different Scenarios

We should consider the multi-path effect on the performance of the mentioned PDOA method in this paper. Fig. 10 shows the positioning error distribution over the indoor room of the three different designs: a) system with no reflections; b) system with reflections; and c) system with reflections by using reflections mitigation scheme [22], [23], where the diffuse channel gain can be measured previously in a certain indoor environment and it can be adopted to mitigate a part of multipath reflections on the performance. From Fig. 10(a), we can see that when there are no reflections in integrated VLCP systems, the positioning errors only come from the thermal noise and shot noise which are small [30], hence most of the positioning errors are below 4 cm. However, this assumption is an ideal scenario, which is not practical where multi-path reflections cannot be avoided.

Fig. 10(b) and (c) show the positioning error distributions over the room with considering the multipath reflections, note that all locations in the room are affected by multipath reflections, especially the corner and edge areas. From Fig. 10(b) and (c), we can find that the positioning errors are low for the most locations, for example, the positioning accuracy performance is quite good at central areas of the indoor room as the multipath reflections of central points of

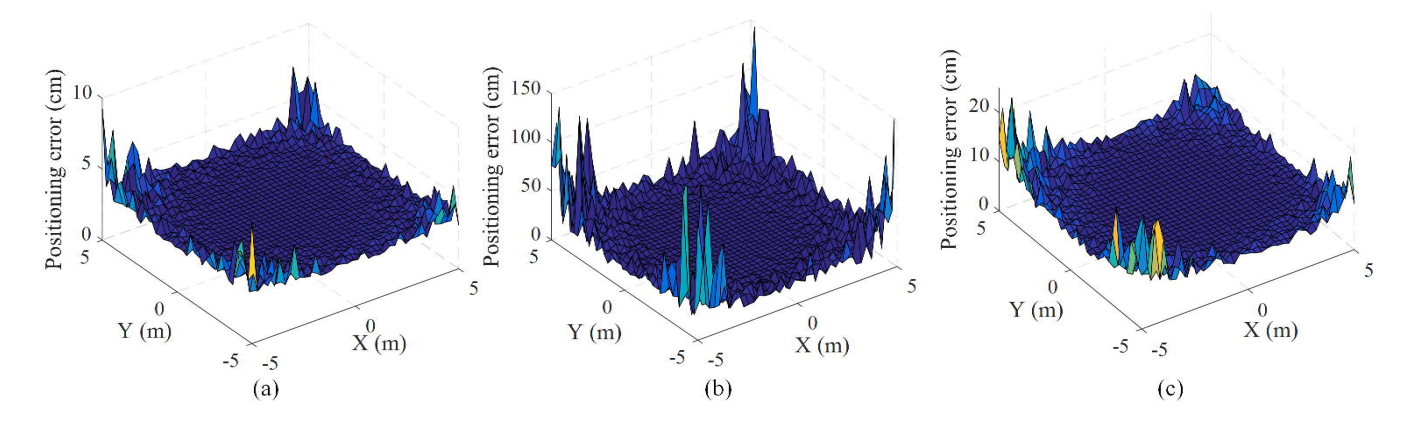


Fig. 10. (a) Positioning error distribution with no reflections; (b) positioning error distribution with reflections; and (c) positioning error distribution with reflections by using reflections mitigation scheme.

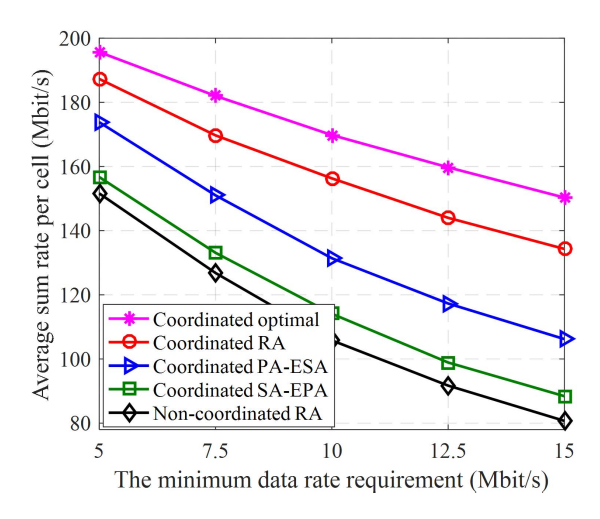


Fig. 11. The performance evaluations vs. the minimum data rate requirement.

the room are weak there. However, positioning errors are high when receivers locate at corners and edges of the indoor room due to the severity of the multipath reflections at corners and edges. Compared with Fig. 10(b), Fig. 10(c) achieves the lower positioning errors, especially the performance advantage is obvious at corner and edge areas. In detail, in Fig. 10(b), most of the positioning errors are below 30 cm at central points, while at corners and edges, the error climbs up to 50 m. By contract, in Fig. 10(c), most of the errors are within 10 cm, and only a few of them are over 10 cm. The worst positioning error is just around 20 cm. This is because that the design in Fig. 10(c) measures the diffuse channel gain previously in a certain indoor environment which can be adopted to mitigate a part of multipath reflections on the performance, hence the positioning accuracy of Fig. 10(c) is not affected significantly by multipath reflections.

In addition, we added a figure to show the relationship between the sum data rate per cell and the minimum data rate requirement, as shown in Fig. 11, in order to indicate the effect of minimum data rate requirement on the performance of the five approaches. From Fig. 11, we can observe that the sum date rate per cell of all approaches decreases with the increase of the minimum data rate requirement. This is because that with the limited spectrum and power resource, the devices with poor channel gains require to be allocated with more resource to guarantee all the minimum data rate requirements of devices. We would like to mention that compared with the proposed coordinated RA approach, the performances of other approaches (except the optimal approach) decrease quickly at the higher minimum data rate requirement region, which indicates that the proposed approach is superior to other approaches under different minimum data rate requirements. The reason is that the proposed coordinated RA approach jointly optimizes the subchannel and power allocation strategy to improve the sum data rate performance.

# VI. CONCLUSION

This paper has investigated the coordinated resource allocation approach in multi-cell integrated VLCP systems to address the joint subcarrier and power allocation problem under the unique optical constraints, the minimum data rate and positioning accuracy requirements of IoT devices. Since the high OOBI significantly degrades both the communication and positioning performance in OFDM-SCM, FBMC-SCM is presented to mitigate OOBI in the integrated multi-cell VLCP system. As the optimization problem is a mixed-integer and NP-hard with non-liner constraints, we decompose it into two subproblems, where a low-complexity suboptimal subcarrier approach is proposed and the SQP method is applied to solve the non-linearly constrained power allocation optimization problem. Numerical results showed that FBMC-SCM can effectively improve the subcarrier utilization by avoiding the need of large GB spacing in comparison to OFDM-SCM in multi-cell integrated VLCP systems. Moreover, the results also verified that the proposed coordinated resource allocation approach can effectively improve the sum rate of devices and the positioning accuracy compared with other resource allocation approaches in multi-cell integrated VLCP systems.

## REFERENCES

 B. Khalfi, B. Hamdaoui, and M. Guizani, "Extracting and exploiting inherent sparsity for efficient IoT support in 5G: Challenges and potential solutions," *IEEE Wireless Commun.*, vol. 24, no. 5, pp. 68–73, Oct. 2017.

- [2] N. Saxena, A. Roy, B. J. R. Sahu, and H. Kim, "Efficient IoT gateway over 5G wireless: A new design with prototype and implementation results," *IEEE Commun. Mag.*, vol. 55, no. 2, pp. 97–105, Feb. 2017.
- [3] M. F. Keskin, A. D. Sezer, and S. Gezici, "Localization via visible light systems," *Proc. IEEE*, vol. 106, no. 6, pp. 1063–1088, Jun. 2018.
- [4] L. Wan, G. Han, L. Shu, S. Chan, and N. Feng, "PD source diagnosis and localization in industrial high-voltage insulation system via multimodal joint sparse representation," *IEEE Trans. Ind. Electron.*, vol. 63, no. 4, pp. 2506–2516, Apr. 2016.
- [5] D. Karunatilaka, F. Zafar, V. Kalavally, and R. Parthiban, "LED based indoor visible light communications: State of the art," *IEEE Commun. Surveys Tuts.*, vol. 17, no. 3, pp. 1649–1678, 3rd Quart., 2015.
- [6] X. Liu, X. Wei, L. Guo, Y. Liu, Q. Song, and A. Jamalipour, "Turning the signal interference into benefits: Towards indoor self-powered visible light communication for IoT devices in industrial radio-hostile environments," *IEEE Access*, vol. 7, pp. 24978–24989, 2019.
- [7] S. Shao, A. Khreishah, and H. Elgala, "Pixelated VLC-backscattering for self-charging indoor IoT devices," *IEEE Photon. Technol. Lett.*, vol. 29, no. 2, pp. 177–180, Jan. 15, 2017.
- [8] G. Pan, H. Lei, Z. Ding, and Q. Ni, "3-D hybrid VLC-RF indoor IoT systems with light energy harvesting," *IEEE Trans. Green Commun. Netw.*, vol. 3, no. 3, pp. 853–865, Sep. 2019.
- [9] Y. Wang, X. Wu, and H. Haas, "Distributed load balancing for Internet of Things by using li-fi and RF hybrid network," in *Proc. IEEE 26th Annu. Int. Symp. Pers., Indoor, Mobile Radio Commun. (PIMRC)*, Hong Kong, Aug. 2015, pp. 1289–1294.
- [10] D. Bykhovsky and S. Arnon, "Multiple access resource allocation invisible light communication systems," *J. Lightw. Technol.*, vol. 32, no. 8, pp. 1594–1600, Apr. 2014.
- [11] F. Jin, R. Zhang, and L. Hanzo, "Resource allocation under delay-guarantee constraints for heterogeneous visible-light and RF femto-cell," *IEEE Trans. Wireless Commun.*, vol. 14, no. 2, pp. 1020–1034, Feb. 2015.
- [12] X. Li, R. Zhang, and L. Hanzo, "Cooperative load balancing in hybrid visible light communications and WiFi," *IEEE Trans. Commun.*, vol. 63, no. 4, pp. 1319–1329, Apr. 2015.
- [13] H. Yang, C. Chen, and W.-D. Zhong, "Cognitive multi-cell visible light communication with hybrid Underlay/Overlay resource allocation," *IEEE Photon. Technol. Lett.*, vol. 30, no. 12, pp. 1135–1138, Jun. 15, 2018.
- [14] X. Zhang, Q. Gao, C. Gong, and Z. Xu, "User grouping and power allocation for NOMA visible light communication multi-cell networks," *IEEE Commun. Lett.*, vol. 21, no. 4, pp. 777–780, Apr. 2017.
- [15] R. Jiang, Q. Wang, H. Haas, and Z. Wang, "Joint user association and power allocation for cell-free visible light communication networks," *IEEE J. Sel. Areas Commun.*, vol. 36, no. 1, pp. 136–148, Jan. 2018.
- [16] S. Shao, A. Khreishah, and I. Khalil, "Enabling real-time indoor tracking of IoT devices through visible light retroreflection," *IEEE Trans. Mobile Comput.*, vol. 19, no. 4, pp. 836–851, Apr. 2020.
- [17] Y. Zhuang, Q. Wang, M. Shi, P. Cao, L. Qi, and J. Yang, "Low-power centimeter-level localization for indoor mobile robots based on ensemble Kalman smoother using received signal strength," *IEEE Internet Things* J., vol. 6, no. 4, pp. 6513–6522, Aug. 2019.
- [18] R. Zhang, W.-D. Zhong, K.-M. Qian, and D.-H. Wu, "Image sensor based visible light positioning system with improved positioning algorithm," *IEEE Access*, vol. 5, pp. 6087–6094, 2018.
- [19] S. Zhang, W.-D. Zhong, P. Du, and C. Chen, "Experimental demonstration of indoor sub-decimeter accuracy VLP system using differential PDOA," *IEEE Photon. Technol. Lett.*, vol. 30, no. 19, pp. 1703–1706, Oct. 1, 2018.
- [20] A. Naz, H. M. Asif, T. Umer, and B.-S. Kim, "PDOA based indoor positioning using visible light communication," *IEEE Access*, vol. 6, pp. 7557–7564, 2018.
- [21] W. Gu, M. Aminikashani, P. Deng, and M. Kavehrad, "Impact of multipath reflections on the performance of indoor visible light positioning systems," *J. Lightw. Technol.*, vol. 34, no. 10, pp. 2578–2587, May 15, 2016.
- [22] X. Zhang, J. Duan, Y. Fu, and A. Shi, "Theoretical accuracy analysis of indoor visible light communication positioning system based on received signal strength indicator," *J. Lightw. Technol.*, vol. 32, no. 21, pp. 4180–4186, Nov. 1, 2014.
- [23] Y. Xu et al., "Accuracy analysis and improvement of visible light positioning based on VLC system using orthogonal frequency division multiple access," Opt. Express, vol. 25, no. 26, p. 32618, Dec. 2017.

- [24] M. F. Keskin, A. D. Sezer, and S. Gezici, "Optimal and robust power allocation for visible light positioning systems under illumination constraints," *IEEE Trans. Commun.*, vol. 67, no. 1, pp. 527–542, Jan. 2019.
- [25] H. Yang, C. Chen, W.-D. Zhong, A. Alphones, S. Zhang, and P. Du, "Resource allocation for multi-user integrated visible light communication and positioning systems," in *Proc. IEEE Int. Conf. Commun. (ICC)*, Shanghai, China, May 2019, pp. 1–6.
- [26] B. Lin, X. Tang, Z. Ghassemlooy, C. Lin, and Y. Li, "Experimental demonstration of an indoor VLC positioning system based on OFDMA," *IEEE Photon. J.*, vol. 9, no. 2, pp. 1–9, Apr. 2017.
- [27] H. Yang, C. Chen, W. Zhong, A. Alphones, S. Zhang, and P. Du, "Demonstration of a quasi-gapless integrated visible light communication and positioning system," *IEEE Photon. Technol. Lett.*, vol. 30, no. 23, pp. 2001–2004, Dec. 2018.
- [28] H. Yang, C. Chen, W.-D. Zhong, and A. Alphones, "Joint precoder and equalizer design for multi-user multi-cell MIMO VLC systems," *IEEE Trans. Veh. Technol.*, vol. 67, no. 12, pp. 11354–11364, Dec. 2018.
- [29] A. T. Hussein, M. T. Alresheedi, and J. M. H. Elmirghani, "20 Gb/s mobile indoor visible light communication system employing beam steering and computer generated holograms," *J. Lightw. Technol.*, vol. 33, no. 24, pp. 5242–5260, Dec. 15, 2015.
- [30] T. Komine and M. Nakagawa, "Fundamental analysis for visible-light communication system using LED lights," *IEEE Trans. Consum. Elec*tron., vol. 50, no. 1, pp. 100–107, Feb. 2004.
- [31] M. Bellanger et al., "FBMC physical layer: A primer," Phydyas, vol. 25, pp. 7–10, Jan. 2010.
- [32] B. Huang, L. Xie, and Z. Yang, "TDOA-based source localization with distance-dependent noises," *IEEE Trans. Wireless Commun.*, vol. 14, no. 1, pp. 468–480, Jan. 2015.
- [33] P. T. Boggs and J. W. Tolle, "Sequential quadratic programming," Acta Numer., vol. 4, pp. 1–51, Jan. 1995.



Helin Yang (Student Member, IEEE) received the B.S. and M.S. degrees from the School of Telecommunications Information Engineering, Chongqing University of Posts and Telecommunications in 2013 and 2016, respectively, and the Ph.D. degree from the School of Electrical and Electronic Engineering, Nanyang Technological University, Singapore, in 2020. His current research interests include wireless communication, visible light communication, the Internet of Things, and resource management. He serves as a Reviewer for

the IEEE international journals, such as the *IEEE Communications Magazine*, IEEE TRANSACTIONS ON WIRELESS COMMUNICATIONS, and the IEEE TRANSACTIONS ON VEHICULAR TECHNOLOGY.



Wen-De Zhong (Senior Member, IEEE) received the B.S. degree from the Beijing University of Posts and Telecommunications, Beijing, China, in1982, and the M.Eng. and Ph.D. degrees from the University of Electro Communications, Tokyo, Japan, in 1990 and 1993, respectively. He is currently a Professor with the School of Electrical and Electronic Engineering, Nanyang Technological University, Singapore. His current research interests include visible light communication/positioning, optical access networks, and signal processing.



Chen Chen (Member, IEEE) received the B.S. and M.Eng. degrees from the University of Electronic Science and Technology of China, Chengdu, China, in 2010 and 2013, respectively, and the Ph.D. degree from Nanyang Technological University, Singapore, in 2017. He is currently a tenured-track Assistant Professor with the School of Microelectronics and Communication Engineering, Chongqing University, China. His research interests include visible light communications, LiFi, visible light positioning, optical access networks, and digital signal processing.



Arokiaswami Alphones (Senior Member, IEEE) received the B.Tech. degree from the Madras Institute of Technology, Chennai, India, in 1982, the M.Tech. degree from the IIT Kharagpur, Kharagpur, India, in 1984, and the Ph.D. degree in optically controlled millimeter wave circuits from the Kyoto Institute of Technology, Kyoto, Japan, in 1992. Since 2001, he has been with the School of Electrical and Electronic Engineering, Nanyang Technological University, Singapore. His current research interests include electromagnetic analysis on planar RF cir-

cuits and integrated optics, microwave photonics, metamaterial-based leaky wave antennas, and wireless power transfer technologies.



Pengfei Du received the B.Eng. degree in mechanical engineering from Sichuan University, Chengdu, China, in 2011, and the Ph.D. degree in optical engineering from Tsinghua University, Beijing, China, in 2016. From 2016 to 2019, he was a Research Fellow with Nanyang Technological University. Since 2019, he has been a Scientist with he A\*STAR's Singapore Institute of Manufacturing Technology (SIMTech). His current research interests include Industrial IoT, lidar, visible light positioning, and quantum detection.



Sheng Zhang received the B.Eng. degree from the School of Optical and Electronic Information, Huazhong University of Science and Technology, China, in 2015. He is currently pursuing the Ph.D. degree with the School of Electrical and Electronic Engineering, Nanyang Technological University, Singapore. He has successfully defended his Ph.D. thesis. His research interests include indoor localization and tracking systems, visible light communication, and positioning.



Xianzhong Xie (Member, IEEE) received the Ph.D. degree in communication and information systems from Xidian University, China, in 2000. He is currently a Professor with the School of Optoelectronic Engineering and the Director of the Chongqing Key Lab of Computer Network and Communication Technology, Chongqing University of Posts and Telecommunications (CQUPT), China. His research interests include MIMO precoding, cognitive radio networks, and cooperative communications.